ELSEVIER

Journal of Nuclear Materials 266–269 (1999) 197–206

journal of nuclear materials

Review of recent works in development and evaluation of high-Z plasma facing materials

Naoaki Yoshida *

Research Institute for Applied Mechanics, Kyushu University, Kasuga, Fukuoka 816, Japan

Abstract

This paper reviews the recent activities and results in development and evaluation of new high-Z materials focusing on tungsten and its alloys. VPS-W coating on graphite and CFC showed superior high heat load properties by inserting sophisticated multilayer diffusion barriers (W/Re) between tungsten and substrate. For successful application it is necessary to know the temperatures for recrystallization and interdiffusion of rhenium and tungsten, which may degrade bonding properties. Sputtering by plasma impurities and damage by energetic charge-exchange neutrals must be considered. Retention of hydrogen isotopes strongly depends on material grade and production process. Dense bubbles and dislocations formed by helium bombardment may act as effective traps for hydrogen. It is anticipated that long range diffusion of helium induces embrittlement. Neutron irradiation is one of the major concerns for tungsten materials in fusion reactor application. The tungsten materials developed so far perform poorly under neutron irradiation and their brittle nature could limit their application as a fusion material. Further efforts are needed to improve ductility while keeping other desirable properties such as high thermal conductivity.

Keywords: High-Z material; Plasma–material interaction

1. Introduction

Plasma facing materials are subjected to very high heat loads from plasma particle bombardment. In the case of D–T burning devices, neutron loading should be taken into account in addition. In order to realize next generation plasma devices and the power reactors in the future, innovative materials for plasma facing components should be developed, that can realize high performance under severe environmental.

Due to their high melting point, low vapor pressure and very low sputtering erosion yield, high-Z materials, especially tungsten and its alloys, are nominated as potential candidates for armor materials of plasma facing components. However, severe plasma contamination can be expected for these impurities. In the case of ITER, for example, tungsten (or its alloys) is designed to be used for divertors, with active R&D being carried on [1,2].

Various kinds of damages of molybdenum and tungsten limiters and divertors have been investigated in hours-long discharges in TRIAM-1M and short pulse discharges in TEXTOR, FTU, ASDEX-Upgrade, Alcator C-Mod. Macroscopic damages on tungsten and molybdenum such as melting and cracking are observed in areas with high heat loads. Microscopic damages such as dislocations in tungsten and molybdenum are observed in TRIAM-1M. Comparative works on these damages with laboratory studies gives a scope of problems to be solved for high-Z plasma facing materials in future.

Numbers of activities have been dedicated to realize high-Z plasma facing components for present and near term experiments in fusion devices. One example is tungsten-coated carbon, which has been utilized in ASDEX-Upgrade. Various techniques such as vacuum plasma spray and chemical vapor deposition have been tried. Both isotropic graphite and CFC were successfully

* Tel.: +81 92 583 7716; fax: +81 92 583 7690; e-mail: yoshida@riam.kyushu-u.ac.jp

0022-3115/99/$ – see front matter
PII: S0022-3115(98)00817-4

coated by tungsten up to 1 mm-thick. Some of the developed materials show good performance with heat loads as high as 10 MW/m^2.

In the last PSI conference in Saint Raphael, impacts of high-Z materials on tokamak plasmas were reviewed in details by N. Noda et al. [3]. In this paper, therefore, present knowledge concerning critical issues of high-Z materials for fusion application will be reviewed and discussed, mainly focusing on tungsten based materials.

2. Properties of tungsten materials and issues as plasma facing materials

The thermal properties of tungsten are first briefly summarized. We have an excellent review of tungsten materials for fusion applications by Smid et al. [4]. Tungsten is a body centered cubic refractory metal with high melting point, 3410°C, and low vapor pressure, 1.3×10^{-7} Pa at melting point. Thermal conductivity is 145 W/mK at room temperature and does not decrease much with increasing temperature. Due to these superior thermal properties, tungsten has been nominated as an armor material for plasma facing components. A critical problem is tungsten's mechanical properties. Although its strength is high enough, its tensile elongation is almost zero at room temperature making it brittle at room temperature. The ductile to brittle transition temperature (DBTT) is far above room temperature at 100°–400°C for pure tungsten. In order to improve this brittleness, several kinds of tungsten based alloys have been developed. It is well known that rhenium additions to tungsten improve the ductility even at lower temperatures. In the case of W-5 wt% Re, for example, DBTT drops to 50°–200°C and still retains fairly high thermal conductivity. La_2O_3 dispersed tungsten alloy (W-1 wt% La_2O_3) is another promising material because of its machinability at room temperature. It has been reported that cast tungsten alloy W–Mo–Y–Ti (W-131) shows some tensile elongation even at 100°C. These alloys are nominated as candidate armor material for ITER divertor plates [1,2].

A critical issue for divertor structure is bonding between the armor and heat sink. In the case of ITER, tungsten or tungsten alloys and copper alloys are proposed as an armor material and heat sink material for divertor plates, respectively. To overcome the large difference in the coefficient of thermal expansion between the two materials (4×10^{-6}/K for tungsten, 1.8×10^{-6}/K for copper), 'brush' structures have been proposed. Three different joining techniques are considered. (1) Plasma spray of Cu or Cu/W to the tip of the W rods. (2) Casting of Cu to the tips of the W rods. (3) Direct diffusion bonding of the W rods to the Cu substrate.

In order to overcome its heavy weight (density = 19.3 g/cm^3), thin tungsten coating on light materials with high thermal conductivity such as copper alloys and graphite are considered as an armor for present and near term fusion devices. Several kinds of coating techniques have been employed for fusion applications; chemical vapor deposition (CVD), physical vapor deposition (PVD), vacuum plasma spray (VPS) and inert gas plasma spray (IPS). Tungsten coatings by CVD and PVD techniques are homogeneous and dense as pure tungsten, whereas those by VPS and IPS are porous (more than 8%) and have texture parallel to the substrate surface, resulting in a significant reduction of thermal conductivity.

The poloidal limiters made of powder metallurgy molybdenum used in TRIAM-1M tokamak for repeating long pulse discharges. The molybdenum initially ductile even at room temperature became brittle by grain growth and recrystallization due to high heat load, resulting in cracking along weakened grain boundaries [5]. These results indicate that the strengthening of grain boundaries and increasing of recrystallization temperature are necessary for fusion applications.

3. Resistance to heat load under normal operation

Under normal operation armor materials of divertor plates suffer long duration heat loading. In the case of ITER, for example, steady state heat load (1000 s) and transient heat load (<10 s) were estimated to be 0.2–5 MW/m^2 and 20 MW/m^2, respectively. The armor materials are required to withstand such heat loads repetitively for several years. Due to the very high melting temperature and very low vapor pressure, tungsten materials can be expected as excellent high heat flux materials. Fujitsuka et al. [6] examined damage of tungsten, W-5 wt% Re and W-25 wt% Re due to high heat load (30 MW/m^2) with long pulse duration (40 s). The weight loss of tungsten and W-5 wt% Re increased linearly with melting time. The weight loss of W-25 wt% Re was several times larger than those of tungsten and W-5 wt% Re. In W-25 wt% Re, due to the low value of its thermal conductivity, the melted area became very thick and this resulted in the large weight loss due to evaporation. These data showed that high concentration W–Re alloys are not favorable as high heat flux materials.

Tungsten coating by plasma spray (PS, 100–550 μm thick) and physical vapor deposition (PVD, 30–200 μm thick) deposited on fine grain graphite tiles were subjected to thermal loads up to 17 MW/m^2 and 2 s pulse duration to establish an experimental data base for ITER and ASDEX Upgrade divertor target plate material [7]. The results proved that PS coatings are capable of withstanding heat loads up to 15 MW/m^2 at 2 s pulse length without any structural changes, and cyclic loading with 1000 cycles at 10 MW/m^2. It was emphasized

that the good performance of PS coatings was related to their porosity, which provided a crack arresting mechanism, and to their mechanical strength, depending on the density of the PS layer. The highly dense PVD coating suffered damage by crack formation at lower heat loads, and thin PVD layers failed under cyclic loading with 1000 cycles at 10 MW/m^2 due to thermal fatigue and melting. The life time of this very thin coating is limited by carbide formation, which leads to a considerable decrease in thermal conductivity, resulting in again higher temperature, grain growth, subsequent embrittlement of the coating and cracking or melting. Tungsten forms tungsten carbide over 1250°C [8] and brittle carbide is produced. Though the PVD coating samples had a re-coating diffusion barrier of about 10 μm thick between the tungsten and the carbon, this was not enough to suppress the diffusion of carbon through it. Recently, PVD coatings on fine graphite and CFC with intermediate W–Re multilayers were successfully developed and their superior heat load properties have been proved [9,10]. Plastic deformation and microcraks due to grain growth by recrystallization were not observed below a surface temperature of about 2200°C, which is about 800°–1000°C higher than recrystallization temperature of powder metallurgy tungsten and carbide formation temperature [10].

4. Resistance to heat load under off-normal operation

Plasma facing components such as the first wall and the divertor will be subjected to severe thermal shocks during off-normal operation such as plasma disruptions (ms time scale) and the vertical displacement events (VDE) occurring on a relatively long time scale (0.3–1 s). Under these events the plasma facing materials will melt and/or evaporate. In spite of the absorption of some part of the incident energy by a dense vapor cloud formed in front of the loaded materials, the remaining fraction of plasma particles penetrate the vapor cloud and cause severe damage such as melt layer removal, recrystallization, grain growth, crack formation and degradation of the bond layer. These material damage have significant impacts on the life time of the components [11].

The effects of plasma disruption and VDE on W materials have been studied extensively. As pointed out by Linke et al. [12] and Akiba et al. [13], heating above DBTT prior to heat load is essential. The irradiation tests of powder metallurgical tungsten specimens were performed with a heat load of 3.2 MJ/m^2 for 1.8 ms at an initial specimen temperature of 25°C (below DBTT) and 650°–700°C (above DBTT). Though a lot of cracks were found at the surface in the low-temperature case, no cracks were observed after the high-temperature irradiation. Above the DBTT (100°–400°C), thermal stress can be reduced by plastic deformation. Gervash et al. [14] investigated the influence of DBTT on tungsten behavior during disruption by using a plasma accelerator. At low heat load (7.5 MJ/m^2, 0.36 ms) and initial temperatures at 330°C (below DBTT) the surface of the specimen is covered by a net of fine surface cracks. A number of large macrocracks also extend through the specimen surface. According to a metallographic cross-section analysis of the heat-loaded specimen, a large number of lateral grain boundary cracks (non-orthogonal the loaded surface) were found. They can cause a loss of thermal conductivity in the surface layer and hence rise serious concerns about the durability of this material. On the contrary, in cases of an initial specimen temperature over DBTT, only a fine surface crack pattern was observed. At an energy deposition of 30 MJ/m^2 significant melting occurs at the surface. In the case of the temperature of the specimens below DBTT, the number of cooling down surface cracks against the background of the wavy resolidified surface can be seen but at the same time no surface cracks were found in case of specimen temperature over DBTT. Decreasing of DBTT is an essential R&D issue for tungsten materials for application as high heat flux materials.

Linke et al. [15] investigated material damage and erosion of alloyed tungsten materials experimentally using short pulse electron beam loading technique. W-5 wt% Re, W-1 wt% La_2O_3, W-30 wt% Cu, which have been suggested as alternative candidates for high heat flux components due to rather good mechanical properties, have been exposed to 5 ms thermal shocks with deposited energy densities up to 12 MJ/m^2. Compared to pure tungsten, the W-5 wt% Re and W-1 wt% La_2O_3 alloys show a rather high tendency to form deep cracks perpendicular to the sample surface. Some of these cracks extend from the loaded surface to the backside of the 5 mm thick specimens. Strong anisotropy in the grain morphology with plate like grains, which orient perpendicular to the specimen surface may be the reason for the tendency to form deep cracks. In the case of W-30 wt% Cu pseudo-alloy, almost no cracks have been generated, but part of the copper was molten and ejected or evaporated due to the low melting point of the copper portions (1080°C).

Disruption damage to plasma facing components and structural materials due to plasma instabilities have been analyzed extensively by Hassanein et al. [11,16,17] using a comprehensive dynamic model. In the analysis, thermal disruption quench times of 0.1–1 ms and plasma energy densities of 10–100 MJ/m^2 are used to evaluate ITER disruption conditions. Among the candidate materials tungsten shows the lowest vaporization losses; less than 1/5 of the losses of carbon. The main reason for the low tungsten erosion rate is its low vapor pressure. Although thermal-quench disruptions have no significant thermal effects on structural materials and coolant

channels, VDEs, in addition to causing severe surface melting and erosion, can result in substantial damage to those components [11,17]. Because of the longer desorption time of VDEs (100–300 ms), much of the plasma incident energy will be conducted through the surface coating material onto the copper structural material and finally to the coolant channels. Fig. 1 [17] shows the temperature of a copper surface at its interface with tungsten or beryllium coating of 5 mm-thick or with 20 mm-thick carbon tiles over 5 mm copper substrate during a typical VDE. In the case of a 5 mm-thick tungsten coating, the copper at interface actually melts. In order to reduce the temperature of the copper surface, thicker coating is required.

5. Effects of particle loads

In the presently operating fusion devices as well as future power reactors, plasma-facing materials will be subjected to high-flux particle bombardment, including ions and neutrals of fuel hydrogen isotope and helium ash, though their flux and energy characteristics depend on the plasma position. In the case of ITER, for example, the flux and average energy of hydrogen ions bombarding divertor plates are estimated to be $<10^{24}$ ions/m^2/s and <100 eV [1]. Therefore one of the main concerns for the divertor materials is sputtering erosion by these high flux ions. The utilization of high-Z materials such as tungsten, which has a high sputtering threshold, has been considered as a possible way of overcoming the sputtering erosion. The situation for the first wall is considerably different from the divertor plate. The flux and energy of hydrogenic species bombarding the first wall of ITER are estimated as $<10^{20}$ particles/m^2/s and 100–500 eV, respectively [1]. These particles are ions and charge-exchange hydrogen neutrals produced in the edge plasma. In addition to these

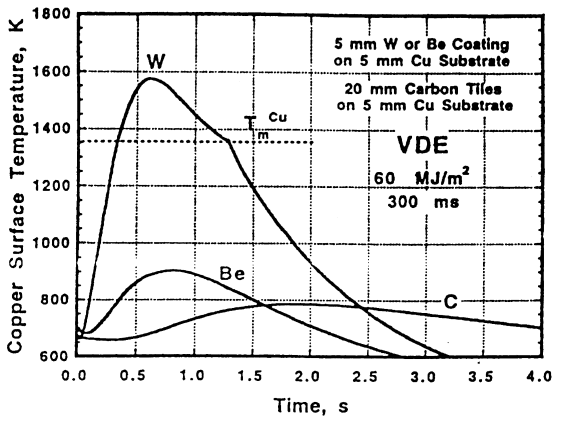

Fig. 1. Rise in copper interface temperature of carbon-, beryllium- and tungsten-coated substrate during a VDE [17].

rather low energy particles, high-energy neutrals escaping from the high temperature core plasma will also impinge on the first wall. Their flux and energy are predicted to be in the order of 10^{18} atoms/m^2/s and 10 keV, respectively. Though the flux of the neutrals to the first wall is much less than that of the ions to the divertor plates, they can result in significant sputtering erosion as well as knock-on damage in the materials. In this section, therefore, recent studies on radiation damage, behavior of implanted hydrogen and sputtering erosion will be reviewed.

5.1. Displacement damage by hydrogen particles

Displacement damage caused by exposing tungsten to tokamak plasmas have been examined by using long duration discharges of TRIAM-1M [18–20]. It was shown that charge-exchange hydrogen neutrals with keV range energies cause significant defects accumulation by displacement damage even in heavy tungsten. Fundamental aspects of radiation damage by hydrogen isotope with keV range energy were investigated by Sakamoto et al. [21,22] by means of hydrogen ion irradiation under in situ transmission electron microscopic observation. Damage evolution shows very clear ion energy dependence; dislocation loops, aggregates of radiation induced interstitial atoms, are formed above 3 keV but not below 2 keV, because the displacement threshold energy is 44 eV [23], which requires hydrogen ions to be higher than 2.05 keV. Not only interstitials but also the same amounts of vacancies are formed by the knock-on damage. According to the numerical calculation using homogeneous reaction kinetics and rate equations by Yoshida et al. [24], the concentration of vacancies in the sub-surface damaged region reaches capacity limit (10^{-3}–10^{-2}) within a very short irradiation period ($<10^{20}$ ions/m^2), because of the very high damage rate and very low mobility of vacancies at the temperature ($E_m^V = 1.7$ eV) [25]. If the hydrogen-vacancy binding energy is high enough, the vacancies are saturated by the implanted hydrogen. Microstructural evolution also depends on irradiation temperature and material purity. Formation of dislocation loops decreases with increasing temperature, while fine cavities of about a few nanometers are slowly formed above 773 K. According to recent experiments at high fluence, dense bubbles are formed even at room temperature by large fluence irradiation above 10^{22} ions/m^2. Dislocation loops, which form dislocation networks at high fluences by interconnection, and bubbles are major defects accumulated by hydrogen ion irradiation.

5.2. Behavior of implanted hydrogen isotopes in tungsten

Retention and permeation of implanted hydrogen isotope is one of the major concerns for plasma facing

materials and have been studied extensively. The behavior of hydrogen isotopes implanted in tungsten materials depends on several factors such as material grade, fabrication process, temperature and ion energy. Fig. 2 shows recent data by Haasz et al. [26] showing retention in tungsten at 300 and 500 K, respectively. In the figures the results of 1 keV D^+ (above the displacement threshold) and 500 eV D^+ (below the displacement threshold) are compared. For fluence $>10^{22}$ D^+/m^2, the reduced energy, and thus the implantation range and displacement damage, does not lead to a reduction in the amount retained. The peak of distribution is well beyond the limit of the implantation range and a long tail extends beyond 500 nm. It must be assumed that significant amount of deuterium has diffused beyond 500 nm. It was also pointed out that tungsten at 500 K had no evidence for saturation. A square root dependence of the retained fluence indicates a diffusion limited trapping mechanism. The distribution of deuterium even at the back surface region (about 0.1% D) indicates implanted deuterium deeply diffused into the materials and uniformly distributed throughout the material. The authors showed that retention of hydrogen isotope in tungsten implanted to high dose (10^{24} D^+/m^2) is maximum (up to 2×10^{20} D/m^2 for 3 keV D_3^+ implantation) at 400–500 K and diminish above 700 K. They also pointed out cumulative fluence in excess of 1×10^{25} D^+/m^2 enhances the retention very much.

It is well known that thermal desorption spectra depend strongly on many factors such as material grade, surface condition, ramping rate and the time between the ion beam termination and the onset of TDS experiment. Because these experimental conditions are different from experiment to experiment, it is not easy to compare the data from different laboratories directly. Nevertheless, Fig. 3 [27] is typical thermal desorption spectra for D_2 release from polycrystalline tungsten following implantation with 3 keV D_3^+ (i.e., 1 keV/D) at 300 K. Ramping rate for these data was about 20 K/s. It is clear that there are three distinct peaks at around 600, 750 and 900 K. The peak temperature depends strongly on ramping rate; in general, it decreases with decreasing ramping rate.

There are many papers discussing the thermal desorption, however the interpretation of responsible hydrogen process for each desorption peak is very contradictory [28–34]. Eleveld et al. [28,29] ascribed the large desorption peak at around 400 K (for 10 K/s) and around 550 K (for 10 K/s) to surface adsorption sites and surface defects caused by deuterium ions such as mono-vacancies and their clusters, respectively. It was also shown that the deuterium trapped by helium bub-

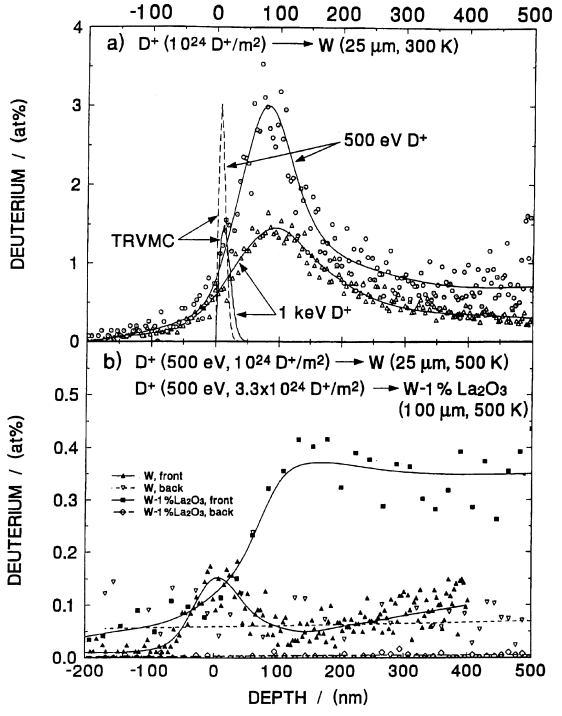

Fig. 2. NRA measurements of the near-surface deuterium depth profiles. (a) 1 keV and 500 eV D^+ implanted into tungsten at 300 K. Implantation profiles are shown for comparison. (b) 500 eV D^+ implantation at 500 K into tungsten and W-1 wt% La_2O_3 [26].

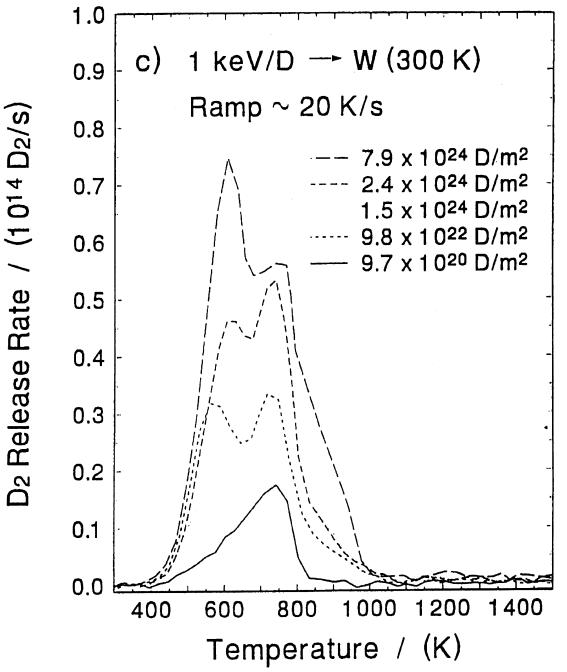

Fig. 3. Thermal desorption spectra for D_2 release from tungsten following implantation with 3 keV D_3^+ at 300 K [27].

bles was released at around 650 K. Pisarev et al. [33] observed four prominent desorption peaks at around 350, 430, 600 and 750 K (for 10 K/s). They ascribed the 350 K peak to detrapping from weak trapping defects such as radiation induced dislocations or blisters. The peaks at 600 and 750 K were ascribed to vacancies and bubbles, respectively. From the comparison of 0.5 keV-D_2^+ irradiation and 8 keV-D_2^+ irradiation, Sakamoto et al. [31] insisted that at rather low fluence ($<10^{22}$ ions/m^2) radiation induced defects, which can be formed only in 8 keV-irradiation, do not affect significantly the retention and desorption of deuterium excepting small desorption at around 710 K (for 1 K/s). The large desorption peaks around 400–650 K (for 1 K/s) could be attributed to weak pre-existing traps such as impurities. Garcia–Rosales et al. [30] and Franzen et al. [34] have investigated the trapping and release of deuterium implanted in tungsten by modeling the results of reemission and desorption experiments. By assuming that the first peak at around 500 K in the TDS spectra (for 5 K/s) is associated with desorption of solute deuterium and deuterium bounded to the low energy natural traps (trapping energy $= 0.5$ eV, concentration $= 6 \times 10^{-3}$ for the single crystal case), then the second peaks near 730 K (for 5 K/s) are dominated by desorption of deuterium bounded to the high energy ion induced traps.

In spite of the large discrepancy among the results reported so far, one could imagine a following picture for the behavior of the implanted hydrogen isotope in tungsten. Some part of hydrogen implanted in the subsurface layer diffuses into the bulk and is trapped by rather weak natural traps with energies of about 0.5 eV. If the ion incident energy is high enough to form radiation damage, some parts of the hydrogen is trapped by ion induced traps such as vacancies, bubbles and dislocations distributing in/near the implantation zone [34]. With increasing implantation temperature, diffusivity of hydrogen increases and results in large and deep retention down to the backward surface as shown in Fig. 2 [26]. At elevated temperatures, diffusion of hydrogen may lead to high and unsaturable inventory at high fluence. In fact, the tungsten coated divertor tiles of ASDEX Upgrade, showed significant amounts of hydrogen diffused into the graphite substrate through plasma sprayed tungsten layer of 0.5 mm [35]. The retained amount of hydrogen, however, decreases drastically for implantation above 600–700 K.

5.3. Retention of hydrogen isotope retention in tungsten based materials

We have discussed hydrogen behavior in rather pure tungsten so far. Tungsten based materials for fusion application such as W-1 wt% La_2O_3, CVD–W, PVD–W, PS–W and mechanically deformed tungsten, have been examined recently. As one can imagine from the results of 'pure tungsten' described above, that the behavior of implanted hydrogen isotope controlled by diffusion and trapping, hydrogen behavior is very material-dependent.

Alimov et al. [36] have investigated deuterium retention in five types of tungsten samples; tungsten single crystal, hot rolled powder metallurgy tungsten, chemical vapor deposited tungsten coating (CVD-W), inert gas plasma sprayed tungsten (IPS-W) and vacuum plasma sprayed tungsten coating (VPS-W). Deuterium retention was measured by means of re-emission (RMS), thermal desorption spectroscopy (TDS) and nuclear reaction analysis (NRA) during and after implantation with 1.5 keV D ions at 300 K. The thermal desorption rate of deuterium depends strongly on the materials. The deuterium desorption from the tungsten single crystal, CVD-W and IPS-W is characterized by a broad temperature range which can be explained by the superposition of two peaks at around 400 K (about 5 K/s) and 690 K (about 5 K/s), respectively, and at about 400 K (about 5 K/s) and 590 K (about 5 K/s) for CVD-W and IPS-W. The thermal release from hot-rolled tungsten shows a broad distribution peaked at around 530 K (about 5 K/s) and a gradual decrease between 700 and 1000 K (about 5 K/s). VPS-W has a sharp thermal release peak at 350 K (about 5 K/s), and small additional peaks at around 950 K (about 5 K/s). Thermal desorption from various tungsten materials was measured up to very high temperature (1473 K) by O'hira et al. recently [37]. As shown in Fig. 4, in an annealed wrought tungsten large desorption peaks around 1100–1500 K (for 0.75 K/s) appears in addition to the 'normal' peak around 500–800 K (0.75 K/s). The high temperature peak, however, diminished in the wrought tungsten annealed at 1773 K for 1 h. The authors pointed out that the thermal desorption of deuterium implanted in the bulk was strongly correlated to change in microstructure

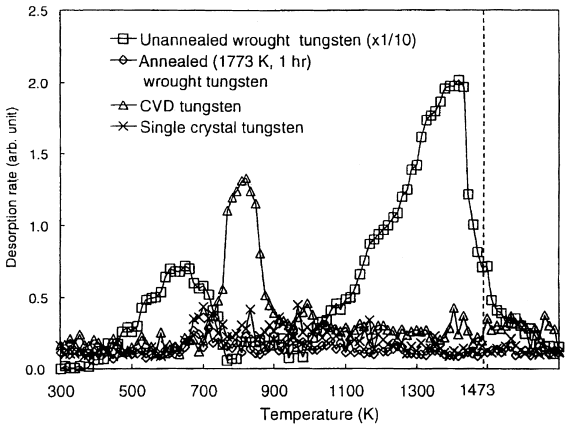

Fig. 4. TDS of deuterium from the various tungsten samples irradiated with 3 keV deuterium ions at 300 K [37].

such as dislocations produced during sample fabrication processes.

Hydrogen permeation properties of plasma-sprayed tungsten (PS-W) coated on steel substrate was investigated by Anderl at al. [38]. Observed permeation rates through composite PS-W/steel composite were several order of magnitudes below the permeation level observed for the sputter-deposited tungsten/steel composite specimen. Characterization analyzes indicated that the plasma-sprayed tungsten had an inhomogeneous microstructure that consisted of splats with columnar solidification, partially melted particles with grain boundaries, and void regions. Reduced permeation levels can be attributed to the complex microstructure and substantial surface-connected porosity.

In order to reveal the hydrogen behavior in the tungsten materials for fusion application in detail, we need further experiments of TDS up to 1500 K or higher, bombardments exceeding 10^{25} ions/m^2, and more knowledge of hydrogen traps in tungsten such as impurities, vacancy clusters, pores, dislocations and grain boundaries.

5.4. Sputtering erosion of tungsten materials

It is widely recognized that the control of impurity generation due to plasma surface interaction is one of critical issues for the presently operating fusion devices as well as future power reactors. Tungsten materials are expected to have low sputtering yields, which could reduce material erosion as well as plasma contamination at relatively low energies around the sputtering threshold energy for deuterium. The erosion behavior of tungsten under oxygen-contaminated deuterium plasma bombardment at 1773 K has been examined by Hirooka et al. [39,40]. The tungsten materials used in these experiments were high-pressure-sintered bulk-material and 1 mm thick coatings on molybdenum prepared by the CVD and PS methods. Despite their low concentration, oxygen-containing plasma impurities dominate the total erosion of tungsten, particularly at relatively low energies below or around the sputtering threshold energy for deuterium, because of the much lower threshold for oxygen sputtering.

One should note that redeposition of tungsten atoms from the plasma and the effect of prompt local redeposition of W^+ ions, which occurs because of the small ratio of ionization length to gyro orbit radius of W^+, reduce the net erosion [41,42]. According to recent DiMES experiments in DIII-D, the net erosion rate of tungsten in the divertor region could be about 200 times lower than that of carbon, indicating that tungsten may be more suitable erosion resistant material for the reactor design [43].

5.5. Effects of helium plasma bombardment

In general, the accumulation of helium is much more harmful to metals than hydrogen because of its strong interaction with lattice defects. It is well known that helium induces embrittlement at high temperature (helium embrittlement). Effects of helium ion bombardment have been studied extensively, emphasizing blistering [44]. Helium enhances the formation of bubbles drastically due to the strong bonding to vacancies and their clusters. As a result, local swelling and degradation of mechanical properties of bulk materials takes place as well. It was reported that a 200 nm thick surface layer damaged by helium ion irradiation can result in embrittlement at low temperatures and ductility loss at high temperatures for a bulk sample of molybdenum [45]. It is anticipated that deep diffusing helium embrittles the bulk materials.

Fig. 5 shows the dependence of the microstructure in molybdenum by 8 keV-He^+ irradiation on irradiation temperature [46]. Interstitial type dislocation loops were formed initially and then bubbles above 1×10^{21} ions/m^2 at all temperatures examined up to 973 K. The local swelling at 1073 K exceeded 50%. The helium implanted subsurface layer exhibites a sponge-like structure. These defects are expected to be good traps for hydrogen [28] and result in hydrogen retention even at elevated temperature. To investigate the effect of these extremely dense defects on mechanical properties, nano-indentation tests were carried out. The relative hardness (Hirr/Hunirr) of the helium-implanted layer becomes about 1.8 by forming of dense dislocation loops and then increases again when the dense fine bubbles are formed at room temperature. Helium ion irradiation changes the subsurface layer as well as properties of bulk; TEM disks of 0.1 mm thick become very brittle by the heavy helium irradiation and can be broken often during handling. As such, irradiation embrittlement occurs for the specimens irradiated not only at room temperature but also at 973 K. Preliminary measurements on heat-loading show that: helium ion bombardment enhances erosion due to synergistic effects of high pressure in the bubbles, degraded the thermal conductivity of the helium injected layer, results in ductility loss, etc. [47]. These results indicate that interaction with helium plasma is a critical issue for metals, especially for high-Z materials such as tungsten and molybdenum in a fusion reactor. We need further investigations on the effects of helium bombardment, especially embrittlement of bulk materials. Synergistic effects with neutron irradiation damage seem important for degradation of mechanical properties and size instability, because helium atoms diffusing deep into bulk affects clustering of radiation induced defects due to strong mutual interaction.

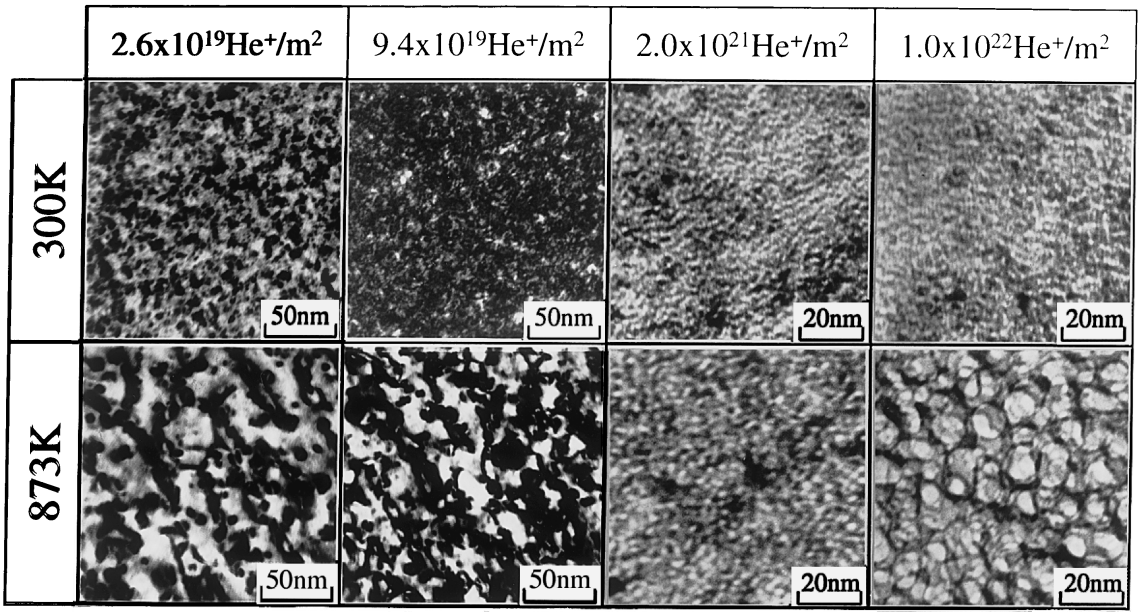

Fig. 5. Microstructural evolution of molybdenum at 300 K and 873 K during irradiation with 8 keV helium ions.

6. Effects of neutron irradiation

In the case of a D–T burning device, in-vessel components will be exposed to considerable neutron irradiation, which induces displacement damage and nuclear transmutation. Flux and fluence of neutrons in ITER during the first phase (basic performance phase), for example, are estimated to be 1 MW/m^2 and 0.4 MWa/m^2, respectively [1]. This means that typical metals will suffer displacement damage of about 1–4 dpa during the phase. The damage during the second phase (enhanced performance phase) expect to be several times higher, and more than one order of magnitude higher for power reactors. It is well known that the displacement damage and nuclear transmutation bring about size instability and degradation of mechanical properties depending on materials and irradiation conditions such as fluence and temperature. A major concern of high-Z materials such as W, Mo and their alloys is neutron irradiation induced embrittlement, i.e. the increase of ductile–brittle transition temperature (DBTT). Abe et al. [48] has investigated neutron irradiation effects on W-26 wt% Re alloys, because the alloying of rhenium improves the ductility very much and moreover large level of rhenium form as solid transmutant in fusion neutron spectra [49]. It was shown, however, that the superior ductility of the alloy vanishes by the rather light damage comparable to the ITER condition. Influence of neutron irradiation on the DBTT of W-10 wt% Re was examined by J.W. Davis [2]. The DBTT increases by about 200°C only by the irradiation of 0.4 dpa at 250°–300°C.

Though neutron irradiation experiments on tungsten materials are very limited so far, there is abundant literature for molybdenum materials, which are good reference for tungsten because their basic material properties are close to each other. Crystal grain size and the heat-treatment are very important factors for radiation induced embrittlement. As reported by Hasegawa et al. [50] and Ueda et al. [51], stress-relived molybdenum (grain size = 2 μm) irradiated at various temperatures from 646 to 1073 K up to rather high dose (6.7–34 dpa) keeps good ductile properties under bending and tensile tests at room temperature, while recrystallized one (grain size = 20 μm) become brittle, with almost no tensile elongation and plastic deformation. Intergranular fractures along weakened grain boundaries due to grain growth lead to poor tensile ductility of the recrystallized molybdenum. Though Mo–Re alloys were developed to improve low temperature ductility and weldability of Mo, the mechanical properties after neutron irradiation are even worse. According to Hasegawa et al. [52,53], stress-relived Mo-5 wt% Re alloy loses ductility at room temperature after the irradiation below 679 K (<27 dpa). In case of Mo-41 wt% Re alloy it becomes very brittle by the irradiation up to 1073 K (maximum examined temperature). Significant radiation induced precipitates may reduce the ductility of high temperature irradiation. Fabritsiev et al. [54] also investigated the neutron irradiation effects on molybdenum and Mo–Re alloys extensively. They showed even worse effects on ductility. Not only molybdenum but also Mo–Re alloys (1,5,9,20 wt% Re) total elongation

reduced to zero by the neutron irradiation between 753–856 K up to 5 dpa.

In order to overcome the low DBTT and the significant embrittlement by recrystallization and neutron irradiation, fine TiC-dispersed molybdenum alloys (Mo-1 wt% TiC) were produced by mechanical alloying treatment [55]. Due to the strengthening of grain boundaries by the dispersed fine TiC particles and very fine grain size (10–400 nm), low temperature toughness as well as irradiation embrittlement improved very much. TiC particles dispersed along grain boundaries reduce grain growth and recrystallization significantly. The recrystallization temperature was about 2273 K, which is 900 K higher than pure Mo. Recently this idea of material design has been applied to W [56].

7. Conclusions

The performance of tungsten materials developed so far for fusion application and direction of future works can be summarized as follows:

1. Development of W and W-based materials

Due to their high melting point, low vapor pressure and low sputtering erosion yield, high-Z materials, especially tungsten and its alloys, are potential candidates for armor materials of plasma facing components. Their brittle nature, however, could limit the application as fusion materials. Many efforts have been dedicated to improve this brittle nature, most of them are still brittle at room temperature except some W–Re alloys. We need further efforts for improving ductility while keeping other desirable properties such as high thermal conductivity.

2. Resistance for heat load under normal and off-normal operations

For steady state high heat load tungsten shows fairly high resistance due to high melting points and good thermal conductivity. VPS-W coating on graphite and CFC showed superior high heat load properties by inserting sophisticated multilayer diffusion barriers (W/Re) between tungsten and substrate to suppress the formation of tungsten carbide. VPS-W looks good from the standpoint of permeation, because the surface connected porosity reduces very deep diffusion into the bulk. For successful application it is necessary to know the temperatures for recrystallization and interdiffusion of rhenium and tungsten, which may induce degradation of mechanical properties of coating and bonding properties. In general, materials have many problems during disruptions and VDEs. To minimize the damage, development of ductile materials and/or operation above the DBTT is necessary.

3. Effects of particle loading (damage, retention, desorption, permeation, sputtering)

Damage and sputtering by plasma particles is significantly lower for tungsten due to high threshold energies for the processes. One should pay attention to sputtering by impurities in plasma and damage by energetic charge-exchange neutrals. The retention of hydrogen isotope strongly depends on material grade and production process, because some kinds of lattice imperfections act as traps for hydrogen and thus modify the diffusion and retention of the implanted hydrogen.

4. Effects of helium bombardment

To date, the effects of implanted helium have been little studied. We should make more clear the role of implanted helium on hydrogen retention and helium embrittlement. Synergistic effects with neutron irradiation damage seem important for degradation of mechanical properties and size instability, because helium atoms diffused deep into the bulk affect clustering of radiation induced defects due to strong mutual interaction.

5. Effects of neutron irradiation

Neutron irradiation is one of the major concerns for tungsten materials for fusion reactor application. The tungsten materials developed so far behave poorly under neutron irradiation. Irradiation embrittlement occurs at rather low dose over a wide range irradiation temperatures.

References

[1] ITER, ITER EDA Document Series, no. 7, IAEA, Vienna, 1996.
[2] J.W. Davis, Development of tungsten structures for use on ITER plasma facing components, JNM (ICFRM-8), to be published.
[3] N. Noda, V. Philipps, R. Neu, J. Nucl. Mater. 241–243 (1997) 227.
[4] I. Smid, M. Akiba, G. Vieider, L.Plöhl, J. Nucl. Mater 258–263 (1998) 160.
[5] N. Yoshida, K. Tokunaga, T. Fujiwara, K. Tawara, T. Muroga, S. Itoh and the TRIAM-group, J. Nucl. Mater., 196–198 (1992) 415.
[6] M. Fujitsuka, I. Mutoh, T. Tanabe, T. Shikama, J. Nucl. Mater. 233–237 (1996) 638.
[7] S. Deschka, C. García-Rosales, W. Hohenauer, R. Duwe, E. Gauthier, J. Linke, M. Lochter, W. Malléner, L. Plöhl, P. Rödhammer, A. Salito, J. Nucl. Mater. 233–237 (1996) 645.
[8] T.B. Massalski (Ed.), Binary alloy phase diagrams, American Society for Metals, Metals Park, Ohio, 1987, p. 599.
[9] H. Maier, S. Kötterl, K. Krieger, R. Neu, M. Balden and the ASDEX Upgrade-team, J. Nucl. Mater. 266–269 (1999) 921.
[10] K. Tokunaga, N. Yoshida, N. Noda, T. Sogabe, T. Kato, J. Nucl. Mater. 258–263 (1998) 998.
[11] A. Hassanein, G. Federici, I. Konkashbaev, A. Zhitlukhin, V. Litunovsky, Materials effects and design implications of disruptions and off-normal events in ITER, Fusion Engineering and Design, to be published.
[12] J. Linke, M. Akiba, H. Bolt, J. van der Laan, H. Nickel, E. van Osch, S. Suzuki, E. Wallura, J. Nucl. Mater. 196–198 (1992) 607.

[13] M. Akiba, H. Madarame, J. Nucl. Mater. 211–215 (1994) 90.
[14] A. Gervash, E. Wallura, I. Ovchinnikov, A.N. Makhankov, J. Linke, G. Breitbach, Fusion Technol. 29 (1996) 499.
[15] J. Linke, R. Duwe, A. Gervash, R.H. Qian, M. Rödig, A. Schuster, J. Nucl. Mater. 258–263 (1998) 634.
[16] A. Hassanein, I. Konkashbaev, J. Nucl. Mater. 233–237 (1996) 713.
[17] A. Hassanein, Fusion Technol. 30 (1996) 713.
[18] K. Tokunaga, T. Muroga, T. Fujiwara, K. Tawara, N. Yoshida, S. Itoh and the TRIAM-group, J. Nucl. Mater., 191–194 (1992) 449.
[19] T. Hirai, K. Tokunaga, T. Fujiwara, N. Yoshida, S. Itoh and the TRIAM-group, J. Nucl. Mater. 258–263 (1998) 1060.
[20] N. Yoshida, Y. Hirooka, J. Nucl. Mater. 258–263 (1998) 173.
[21] R. Sakamoto, T. Muroga, N. Yoshida, J. Nucl. Mater. 212–215 (1994) 1426.
[22] R. Sakamoto, T. Muroga, N. Yoshida, J. Nucl. Mater. 220–222 (1995) 819.
[23] P. Lucasson, Fundamental aspects of radiation damage in metals, vol. 1, CONF751006-P1, M.T. Robinson and F.W. Young, Jr. (Eds), USERDA, 1975, p. 42.
[24] N. Yoshida, R. Sakamoto, J. Nucl. Mater. 251 (1997) 284.
[25] M.W. Thompson, Philos. Mag. 5 (1969) 278.
[26] A.A. Haasz, J.W. Davis, M. Poon, R.G. Macaulay-Newcombe, J. Nucl. Mater. 258–263 (1998) 889.
[27] A.A. Haasz, J.W. Davis, J. Nucl. Mater. 241–243 (1997) 1076.
[28] H. Eleveld, A. van Veen, J. Nucl. Mater. 191–194 (1992) 433.
[29] H. Eleveld, A. van Veen, J. Nucl. Mater. 212–215 (1994) 1421.
[30] C. Garcìa-Rosales, P. Franzen, H. Plank, J. Roth, E. Gauthier, J. Nucl. Mater. 233–237 (1996) 803.
[31] R. Sakamoto, T. Muroga, N. Yoshida, J. Nucl. Mater. 233–237 (1996) 776.
[32] A.P. Zakharov, A.E. Gorodetsky, V.Kh. Alimov, S.L. Kanashenko, A.V. Markin, J. Nucl. Mater. 241–243 (1997) 52.
[33] A.A. Pisarev, A.V. Varava, S.K. Zhdanov, J. Nucl. Mater. 220–222 (1995) 926.
[34] P. Franzen, C. Garcia-Rosales, H. Plank, V.Kh. Alimov, J. Nucl. Mater. 241–243 (1997) 1082.
[35] P. Franzen, H. Maier, D. Schleuflner, R. Behrisch, M. Balden, and the ASDEX Upgrade team, 24th Euro. Conf. on Contr. Fusion and Plasma Phys., Berchtesgaden, 1997, European Physical Society, to be published.
[36] V.Kh. Alimov, B.M.U. Scherzer, J. Nucl. Mater. 240 (1996) 75.
[37] S. O'hira, A. Steinér, H. Nakamura, R. Causey, M. Nishi, S. Willms, J. Nucl. Mater. 258–263 (1998) 990.
[38] R.A. Anderl, R.J. Pawelko, M.R. Hankins, G.R. Longhurst, R.A. Neiser, J. Nucl. Mater. 212–215 (1994) 1416.
[39] Y. Hirooka, M. Bourham, J.N. Brooks, R.A. Causey, G. Chevalier, R.W. Conn, W.H. Eddy, J. Gilligan, M. Khandagle, Y. Ra, J. Nucl. Mater. 196–198 (1992) 149.
[40] Y. Hirooka, Physica Scripta T64 (1996) 84.
[41] D. Naujoks, et al., Nucl. Fusion 36 (1996) 671.
[42] K. Krieger, H. Maier, V. Rohde, K. Asmussen, M. Balden, D. Coster, J. Roth, R. Schneider, A. Thoma, and the ASDEX Upgrade-Team, Proc. 24th Euro. Con. Contr. Fusion and Plasma Phys., Berchtesgaden, 1997, European Physical Society, to be published.
[43] C.P.C. Wong, D.G. Whyte, R.J. Bastasz, J. Brooks, W.P. West, W.R. Wampler, J. Nucl. Mater. 258–263 (1998) 433.
[44] M. Kaminsky, Radiation Effects on Solid Surfaces, American Chemical Society, Washington, DC, 1976.
[45] K. Shinohara, A. Kawakami, S. Kitajima, Y. Nakamura, M. Kutsuwada, J. Nucl. Mater. 179–181 (1991) 246.
[46] H. Iwakiri, H. Wakimoto, H. Watanabe, N. Yoshida, J. Nucl. Mater. 258–263 (1998) 873.
[47] K. Makise, private communication, 1998.
[48] K. Abe, private communication, 1996.
[49] L.R. Greemwood, F.A. Gerner, J. Nucl. Mater. 212–215 (1994) 635.
[50] A. Hasegawa, K. Abe, M. Satou, K. Ueda, C. Namba, J. Nucl. Mater. 233–237 (1996) 565.
[51] K. Ueda, M. Satou, A. Hasegawa, K. Abe, Sci. Rep. RITU, part A, 45 (1997) 163.
[52] A. Hasegawa, K. Abe, M. Satou, C. Namba, J. Nucl. Mater. 225 (1995) 259.
[53] A. Hasegawa, K. Ueda, M. Satou, K. Abe, J. Nucl. Mater. 258–263 (1998) 902.
[54] S.A. Fabritsiev, A.S. Pokrovsky, J. Nucl. Mater. 252 (1998) 216.
[55] Y. Kitsunai, H. Kurishita, M. Narui, H. Kayano, Y. Hiraoka, J. Nucl. Mater. 239 (1996) 253.
[56] Y. Kitsunai, H. Kurishita, H. Kayano, Y. Hiraoka, T. Igarashi, T. Takida, Microstructure and impact properties of ultra-fine grained tungsten alloys dispersed with TiC, J. Nucl. Mater. 271&272 (1999) in press.